

Evidence for drift waves in the turbulence of reversed field pinch plasmas

D. J. Thuecks, A. F. Almagri, J. S. Sarff, and P. W. Terry

Citation: *Physics of Plasmas* **24**, 022309 (2017); doi: 10.1063/1.4976838

View online: <http://dx.doi.org/10.1063/1.4976838>

View Table of Contents: <http://aip.scitation.org/toc/php/24/2>

Published by the *American Institute of Physics*



Small Conferences. BIG Ideas.

Applied Physics
Reviews

SAVE THE DATE!
3D Bioprinting: Physical and Chemical Processes
May 2–3, 2017 • Winston Salem, NC, USA

The background of the banner features a blue-toned image of a human hand holding a glowing, blue, branching structure that resembles a biological or chemical process, possibly related to bioprinting or plasma physics.

Evidence for drift waves in the turbulence of reversed field pinch plasmas

D. J. Thuecks,^{1,2,3,a)} A. F. Almagri,^{1,2} J. S. Sarff,^{1,2} and P. W. Terry^{1,2}

¹*Department of Physics, University of Wisconsin-Madison, 1150 University Avenue, Madison, Wisconsin 53706, USA*

²*Center for Magnetic Self-Organization in Laboratory and Astrophysical Plasmas, Madison, Wisconsin 53706, USA*

³*Department of Physics, Washington College, 300 Washington Avenue, Chestertown, Maryland 21620, USA*

(Received 12 October 2016; accepted 6 February 2017; published online 22 February 2017)

A detailed characterization of the high-frequency range of the fluctuation spectrum in reversed field pinch plasmas is presented, revealing a variety of new features distinct from global tearing modes and the cascade that they are thought to drive. The anisotropic broadband spectrum of the fluctuating electric field is measured. The power in the fluctuating kinetic energy $(1/2)m_i n_i \tilde{V}_{\mathbf{E} \times \mathbf{B}_0}^2$, previously measured to be smaller than the magnetic energy in the tearing-mode-unstable frequency range, becomes greater than and diverges from the magnetic energy above 60–80 kHz. The lack of equipartition at high frequencies coincides with the measured signatures of the independent fluctuation activity broadly consistent with the drift-wave fluctuations. Statistical coherence measurements reveal the mode activity that is compressive with a large amplitude in the vicinity of strong density gradients and with a phase speed comparable to the electron drift speed. There is a distinct high-frequency correlation between the fluctuations of density and the parallel magnetic field. Elevated coherences associated with this fluctuation feature return more quickly after a sawtooth event than the corresponding coherences associated with tearing activity. *Published by AIP Publishing.*

[<http://dx.doi.org/10.1063/1.4976838>]

I. INTRODUCTION

Turbulence is present in a variety of laboratory and space plasmas and provides a means by which energy deposited at one spatial scale can be transferred to other scales. Collective plasma motion with wavenumbers other than those at which energy is injected by instability are excited through nonlinear energy transfer and can contribute to particle and energy transport. In the standard view of turbulence, energy is dissipated at the smallest scales resulting in plasma heating.

In reversed field pinch (RFP) plasmas undergoing strong magnetic relaxation, energy is deposited into large-scale fluctuations by unstable tearing modes. A nonlinear energy cascade transfers the tearing-scale energy to a range of smaller scales, resulting in a broadband fluctuation power spectrum. The relaxation process happens through quasi-periodic magnetic reconnection events called sawteeth due to the temporal variation displayed in the mean-field quantities.^{1–4} Magnetic turbulence driven by tearing modes is a significant contributor to transport in standard RFP plasmas.

Previous detailed measurements of the magnetic turbulence in the edge region of Madison Symmetric Torus (MST) standard RFP plasmas reveal key properties of the turbulent cascade.⁴ The power spectrum is anisotropic relative to the strong, mean magnetic field \mathbf{B}_0 , with the fluctuation energy spread broadly in wavenumbers perpendicular to \mathbf{B}_0 . This anisotropy is present for frequencies above those associated with tearing modes (≈ 10 – 20 kHz) and extends beyond the ion cyclotron frequency (≈ 600 kHz), reaching a spectral range where kinetic effects likely become important. The anisotropy suggests that the high-frequency fluctuations

are associated with modes localized perpendicular to the magnetic field. Coherence and phase measurements confirm this result and indicate a standing-wave structure for these smaller-scale fluctuations that is reminiscent of collisional shear Alfvén wave and microtearing mode structures.⁴

Many theoretical models and simulations, starting with Iroshnikov⁵ and Kraichnan⁶ and continuing to the present,^{7–10} treat MHD plasma turbulence as a cascade carried by Alfvénic fluctuations. The focus on Alfvénic turbulence arises in part because of the prevalence of Alfvén waves in magnetized plasmas for scales larger than an ion gyroradius. Given that magnetic turbulence in MST originates in global scales from tearing instability, it is reasonable to hypothesize that the broadband turbulence in MST is Alfvénic in character, albeit with features associated with confining geometry and magnetic configuration. A key property of an Alfvénic cascade is the equipartition of the magnetic and kinetic energy in the inertial range of the turbulence.

In this paper, we examine the electrostatic component of the turbulence to better characterize turbulent modes in MST plasmas. We show that electric field fluctuations are anisotropic and are driven in part by energy deposited into the tearing modes. Despite this, we find that the magnetic and kinetic energies in the turbulence are not in equipartition. Electric field spectra are less steep than their magnetic counterpart, which suggests the presence of an additional energy source for electric field (kinetic energy) fluctuations. Statistical analysis techniques identify a previously unobserved mode with characteristics that are consistent with general drift wave theory. Coherence and phase measurements indicate that the drift mode is compressive with a phase velocity comparable to the electron drift speed. The coherence is highest where the density gradient is largest.

^{a)}Electronic mail: dthuecks2@washcoll.edu

Recently, improved theoretical understanding of drift waves in RFP plasmas has emerged through gyrokinetic modeling of less turbulent operating regimes that have greatly reduced tearing activity and improved confinement. These regimes include inductive current profile control¹¹ and quasi-single-helicity self-organization (quasi-single helicity and single-helical-axis states, or QSH¹² and SHAx,¹³ respectively). With the reduction of tearing modes, it is important to identify other types of fluctuations and instabilities that contribute to turbulence and transport beyond that associated with tearing modes. In particular, the stability of ion-temperature-gradient (ITG), trapped-electron mode (TEM), and microtearing modes have been investigated analytically and numerically.^{14–19} Comparisons of experimental measurements with comprehensive gyrokinetic models that use experimental equilibria for several of these improved-confinement cases have confirmed the presence of microtearing modes,²⁰ TEM, and ITG turbulence.²¹

It should also be noted that many of the observed features presented in this paper are similar to features seen in the space turbulence. In particular, solar wind turbulence has been shown to be anisotropic with respect to a local magnetic field.^{22,23} Despite solar wind turbulence being primarily Alfvénic, observations have shown a small but unmistakable lack of equipartition between magnetic and kinetic fluctuation energies.^{24–27} Additionally, compressive wave modes (such as the slow MHD wave) contribute to solar wind turbulence and may be an important factor in explaining observed properties of the turbulent cascade.²⁸ As a result, the observations presented here can contribute to our understanding of turbulence observed in space and laboratory astrophysics experiments.

The organization of this paper is as follows. Section II will describe our experimental design. Section III will present basic characteristics of electric field fluctuations and examine energy partition between kinetic and magnetic fluctuations. Section IV presents statistical coherence measurements between fluctuating quantities that are used to identify a drift wave mode that is present at high frequencies.

II. EXPERIMENTAL DESIGN

The MST device produces RFP plasmas with major radius $R = 1.5$ m and minor radius $a = 0.50$ m. The mean, equilibrium magnetic field in an RFP plasma has very strong shear in the radial direction; the magnetic field is dominantly toroidal in the core, becomes purely poloidal at the magnetic reversal surface (at radial location $r/a \approx 0.85$ for plasmas discussed here), and acquires a small negative component in the toroidal direction in the extreme edge.

Quasi-periodic impulsive magnetic reconnection events (sawteeth) have a large influence on both plasma turbulence and mean-field dynamics. They are driven by several linearly unstable core-resonant tearing modes (with poloidal mode number $m = 1$ and toroidal mode number $n \sim 2R/a$) and serve as the main avenue for magnetic relaxation in RFP plasmas. During this relaxation process, nonlinear interactions energize linearly stable $m = 0$ modes resonant at the magnetic reversal surface, stable $m = 1$ modes with $n \geq 2R/a$, and

stable $m \geq 2$ modes with $|n| \gg 2R/a$.²⁹ These interactions are responsible for the creation of a mean-field dynamo emf that regulates the current density profile as well as an energy cascade to small-scale structures.

Measurements of plasma turbulence reported here were obtained with insertable probes in the edge region of low-current ($I_p \approx 200$ kA) discharges. Probe insertion ranged from $r/a = 0.77$ (inside the magnetic reversal surface) out to the chamber wall at $r/a = 1.0$. Typical local plasma parameters are density $n_e \sim 1\text{--}5 \times 10^{12}$ cm⁻³, temperatures $T_e \sim T_i \leq 50$ eV, and volume-average mean magnetic field $|\mathbf{B}_0| \approx 1100$ G. The probes incorporated multiple surface electrodes and internal three-dimensional \hat{B} -cubes, allowing simultaneous measurements of the floating potential V_f , ion saturation current J_s , electric field \mathbf{E} , and magnetic field \mathbf{B} , in close spatial proximity. Signals from these probes were digitized at 6 MHz, and the analysis was limited to data taken during the plasma current flattop in the timescale 20 ms–38 ms (Fig. 1(a)). The temporal behavior of fluctuations is examined with respect to the sawtooth cycle (seen most clearly in Fig. 1(b)), with datasets from several sawteeth in multiple shots sliced into short time series centered around the sawtooth crash. Figure 1(c) shows a narrowed view of two sawtooth events while Fig. 1(d) shows the accompanying \tilde{V}_f signals. Natural plasma rotation ensures

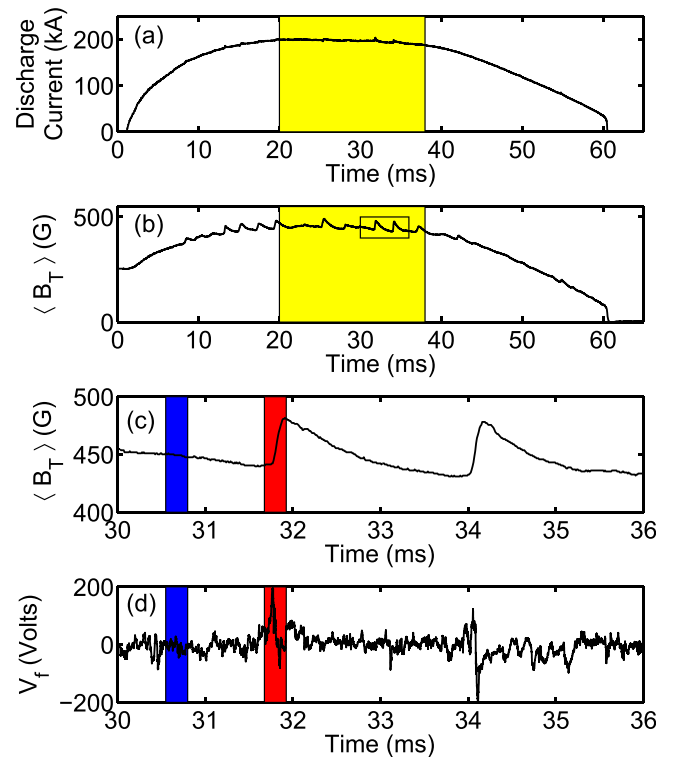


FIG. 1. (a) The plasma current for a complete discharge. The analysis was restricted to the flattop region from 20 ms to 38 ms (shaded). (b) Sawtooth behavior is most evident in $\langle B_T \rangle$, the toroidal magnetic field averaged over the poloidal cross section. The small box in (b) represents the plot region presented in (c), which provides a zoomed view of two sawtooth cycles. The \tilde{V}_f series associated with these two sawtooth events is shown in (d). The blue and red shaded regions in (c) and (d) show how the labels “between” and “during” sawteeth are defined for a given sawtooth event; “between” (blue) represents data averaged in a window from 1.25 ms to 1.0 ms before a sawtooth crash and “during” (red) represents data averaged over a window of 0.25 ms spanning a sawtooth crash.

that sawtooth ensembles constructed in this way approximate spatial averages over magnetic flux surfaces.

Measurements of the equilibrium magnetic field were acquired from a subset of \hat{B} -cubes using analog integrators with the bandwidth ≤ 250 kHz. For measuring the high-frequency fluctuations, the magnetic signals from the remaining \hat{B} -cubes were differentially amplified with the bandwidth ≤ 3 MHz. Electrode-based signals were measured using isolation amplifiers, and all measurements had a bandwidth of at least 1 MHz. When measuring the ion saturation current for plasma density, electrode pairs were used as double Langmuir probes with a 200 V bias potential between electrodes, approximately four times greater than the local T_e .

Conventional FFT-based techniques were used to produce auto- and cross-power fluctuation spectral densities, coherences, and phase differences between measured quantities as a function of frequency. An extension of a two-point correlation technique³⁰ was used to estimate the two-dimensional power spectral density $S_E(k_p, k_t)$ of the electric field fluctuations, where k_p and k_t represent poloidal and toroidal wavenumbers, respectively. Three V_f measurements in an “L”-shaped configuration (spaced poloidally and toroidally) were used to estimate $S_E(k_p, k_t)$ using the relationship $\mathbf{E}(\mathbf{k}, \omega) \approx -i\mathbf{k}V_f(\mathbf{k}, \omega)$. From $S_E(k_p, k_t)$, one-dimensional power spectral densities of electric field fluctuations were found by integrating with respect to the second wavenumber. A further extension to this technique allowed coherences as a function of frequency and wavenumber to be measured. The two-point correlation technique and associated extensions are described in an appendix in the [supplementary material](#).

III. ELECTRIC FIELD SPECTRA AND ENERGY PARTITION

The power spectral densities $S_E(\omega)$ and $S_E(k_\perp)$ associated with the electric field fluctuations are shown in Fig. 2, where ω is the wave frequency and k_\perp is the wavenumber perpendicular to the local mean magnetic field. A broadband spectrum is observed in both plots. The rise and fall of the power spectrum through a sawtooth cycle provides evidence for a connection between the tearing magnetic reconnection and electric field fluctuations. In Fig. 2, “Between” represents data averaged in a window from 1.25 ms to 1.0 ms before a sawtooth crash, and “During” represents data averaged over a window of 0.25 ms centered on a sawtooth crash (as illustrated in Figs. 1(c) and 1(d)). This rise and fall seen across all frequencies and a broad range of wavenumbers has been observed in magnetic fluctuations by Ren *et al.*⁴ and is evocative of a nonlinear energy cascade as described by Sarff *et al.*³¹ as well as the presence of a coupling mechanism between magnetic and electric field fluctuations. Figure 3 shows a scaling that corresponds to a power law $k^{-\alpha}$ with $\alpha = 1.55 \pm 0.15$. This spectral index is roughly consistent with solar wind results, though this fit is performed over less than an order of magnitude in wavenumbers and is unable to distinguish between Kolmogorov (5/3) and Kraichnan (3/2) scalings.^{6,24,32}

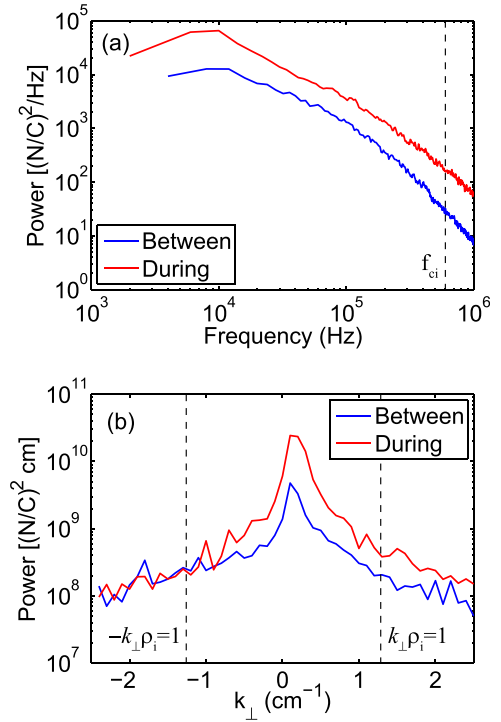


FIG. 2. Power spectral densities (a) $S_E(\omega)$ and (b) $S_E(k_\perp)$ associated with electric field fluctuations. During impulsive reconnection events, power rises at all frequencies, indicative of a nonlinear energy cascade from tearing-mode frequencies to higher frequency fluctuations. For reference, the cyclotron frequency for majority ions is $f_{ci} \approx 600$ kHz.

Electric field fluctuations exhibit strong wavevector anisotropy as seen in the two-dimensional power spectral densities in Fig. 4. The electric field fluctuation anisotropy is very narrow and remains aligned along a direction perpendicular to \mathbf{B}_0 , even as the field direction changes with the radial location. (The solid black lines in Fig. 4 identify $\mathbf{k} \cdot \mathbf{B}_0 = 0$.) These observations imply a relatively short coherence length associated with the electric field fluctuations, very similar to previous measurements for high-frequency magnetic fluctuations where short radial coherence lengths were explicitly measured.⁴ One difference that has been observed for the anisotropic electric field fluctuations as compared with the anisotropy of the magnetic fluctuations is that the electric field anisotropy persists at low

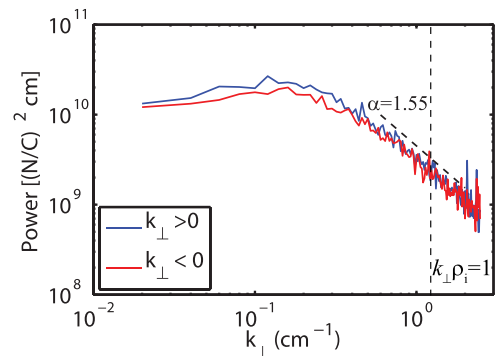


FIG. 3. Power spectral density of electric field fluctuations as a function of k_\perp . For high wavenumbers, spectra in both directions scale like power laws with $\alpha = 1.55 \pm 0.15$.

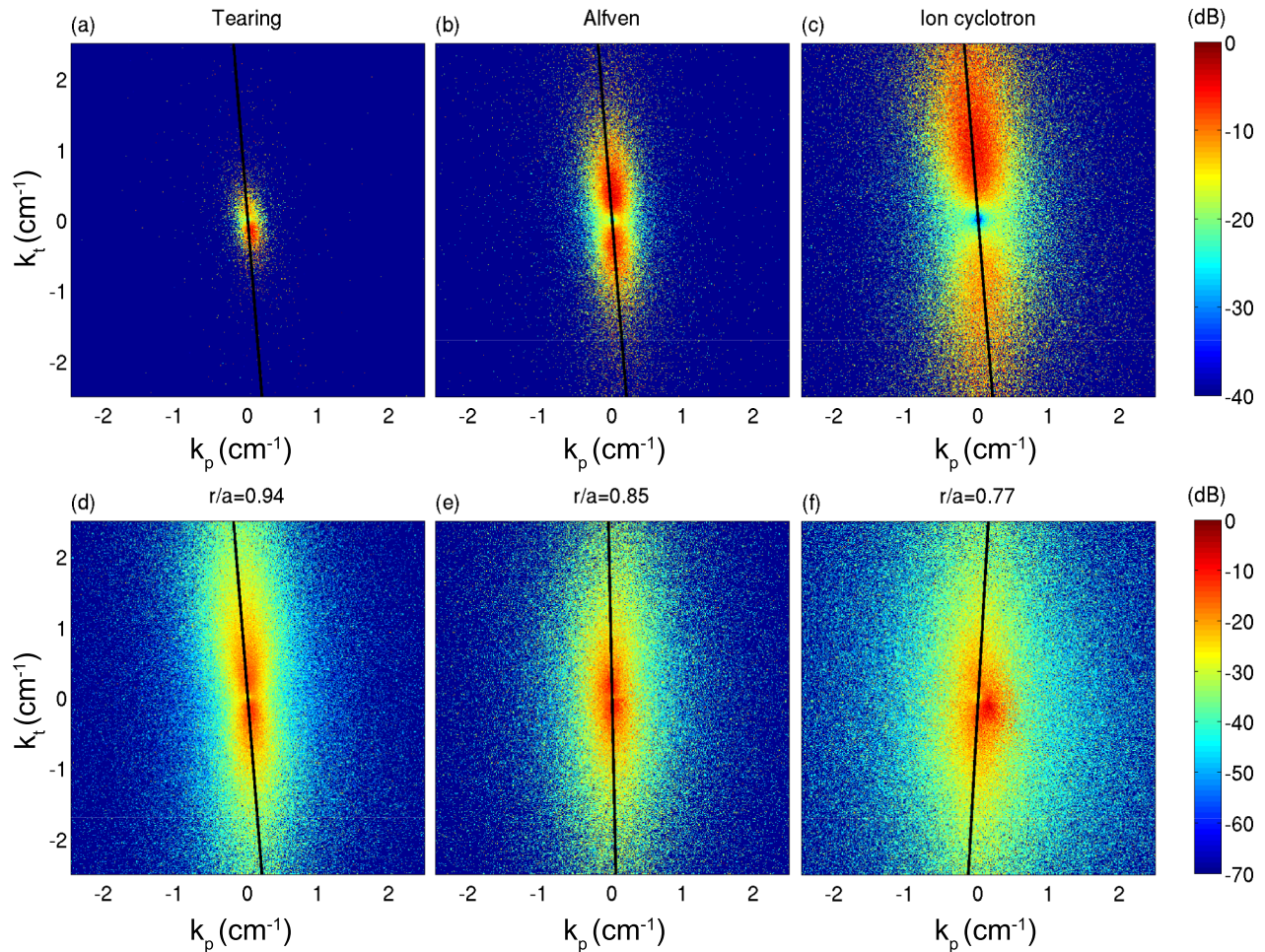


FIG. 4. Plots of $S_E(k_p, k_t)$ reveal that electric field fluctuations are strongly anisotropic. Power is spread broadly in a direction perpendicular to the local mean magnetic field (the solid black line identifies $\mathbf{k} \cdot \mathbf{B} = 0$), while it is spread narrowly in the parallel direction. Panels (a)–(c) were measured at $r/a = 0.94$ and show that this anisotropy is present at frequencies associated with the tearing mode activity (5 kHz–20 kHz), frequencies where Alfvén activity is most likely (50 kHz–200 kHz), and frequencies near the ion cyclotron frequency (400 kHz–800 kHz). Panels (d)–(f) (which include frequencies above 5 kHz) show that this anisotropy tracks the mean magnetic field direction as it changes with radial location, indicating a short radial coherence length for electric field fluctuations. In (a)–(c), each spectrum has been normalized to its peak value. In (d)–(f), each spectrum has been normalized to the overall maximum value.

(tearing mode) frequencies, likely indicating that the radial coherence lengths of electric field fluctuations at these scales are shorter than those associated with the global tearing mode structure.^{1,4} It also appears from Fig. 4 that the width of the toroidal mode number spectrum (i.e., the extent of the strong signal along the solid black line) becomes smaller for inner radii, while this quantity shows little change in the magnetic fluctuation spectrum.

The electric field fluctuations are associated with $\tilde{\mathbf{E}} \times \mathbf{B}_0$ flow, allowing evaluation of the turbulent kinetic energy using \tilde{E}_r , \tilde{E}_t , and B_{0p} (since $B_{0p} \gg B_{0r}, B_{0\theta}$). The energy density contained in magnetic and kinetic fluctuations are directly compared in Fig. 5, which reveals a lack of energy equipartition. At low frequencies, the magnetic energy dominates the power spectrum, as expected, for global tearing modes. The slopes of the two spectra are quite different with increasing frequency, and the kinetic energy becomes dominant near 60 kHz. The cross-over frequency depends on the local plasma density, and while the local value $n_e \approx 2 \times 10^{12} \text{ cm}^{-3}$ measured with a triple Langmuir probe is used here, there is some uncertainty in the cross-over frequency because

the density gradient scale length in the edge region is comparable to the radial coherence length of the fluctuations. The lack of energy equipartition at larger frequencies suggests the emergence of non-Alfvénic modes at small scale, which is discussed in Section IV.

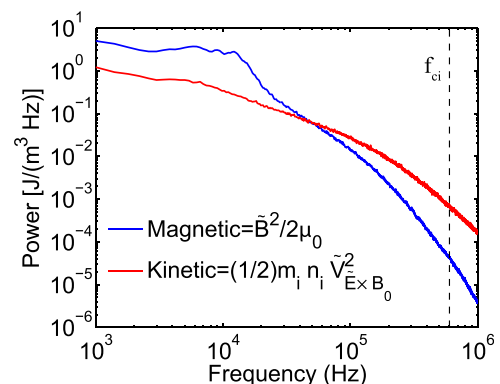


FIG. 5. Partition of energy between kinetic and magnetic fluctuations for $r/a = 0.85$. The residual energy $E_r(\omega) = E_b(\omega) - E_k(\omega) > 0$ at low frequencies, while $E_r(\omega) < 0$ at frequencies above ≈ 60 kHz.

The prevalence of Alfvén waves in magnetized plasmas for frequencies below the ion cyclotron frequency make them a natural choice for describing the nature of MHD turbulence,^{5,6} and energy equipartition is intrinsic to Alfvén models of turbulence. Nevertheless, a small but unmistakable lack of equipartition between magnetic and kinetic fluctuation energies has been observed in solar wind turbulence,^{24–27} despite the Alfvénic nature of these fluctuations. These measurements of solar wind turbulence show that magnetic spectra are somewhat steeper than kinetic spectra. This is the same trend observed in MST plasmas, although the difference between spectral indices in the solar wind is in the order of 10%, whereas here, it is roughly a factor of two. The degree of equipartition violation is characterized by the residual energy $E_r(k) = E_v(k) - E_b(k)$, i.e., the difference in energies for kinetic $E_v(k)$ and magnetic $E_b(k)$ fluctuations, and is a current topic of theoretical research.²⁷

IV. STATISTICAL COHERENCE MEASUREMENTS

Statistical analysis of the measured electrostatic and magnetic fluctuations reveals distinguishing characteristics of the waves or instabilities in the broadband turbulence. These characteristics suggest that drift waves may be excited in the turbulence, either by coupling to the tearing-driven cascade or through instability. Figure 6 shows the coherence and cross phase between electron density fluctuations, \tilde{n}_e , and floating potential fluctuations, \tilde{V}_f . Two features stand out in the coherence spectrum. The low frequency feature from 5 to 20 kHz is associated with the dominant tearing modes. A second feature has its peak near 80 kHz and extends over several hundred kHz. Figure 6(b) reveals a cross phase between \tilde{n}_e and \tilde{V}_f that is near zero in this higher frequency range. The amplitudes of V_f and n_e fluctuations have been compared, revealing that $(e\tilde{V}_f/k_B T_e)/(\tilde{n}_e/n_e) \approx 0.8$ for these high frequency fluctuations (signals were

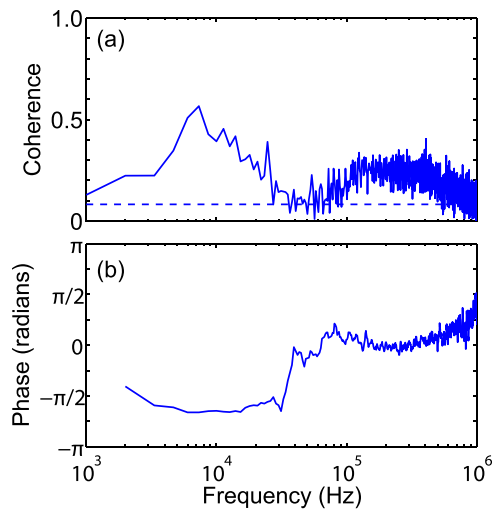


FIG. 6. Coherence and cross phase between \tilde{V}_f and \tilde{n}_e at $r/a = 0.85$. Measurements reveal a high degree of coherence between \tilde{n}_e and \tilde{V}_f near 20 kHz, corresponding to tearing mode activity. A second peak is apparent at high frequencies near 80 kHz and extending for several hundred kHz. A cross phase near zero in this high frequency band is consistent with the behavior of drift waves. The dashed line in (a) represents the statistical noise floor.

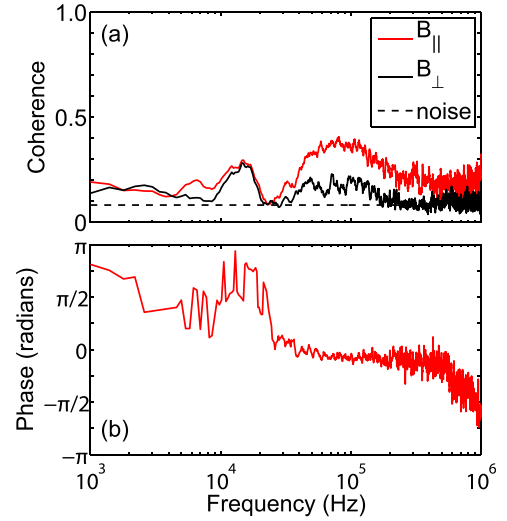


FIG. 7. (a) Coherence and (b) phase have been measured between \tilde{n}_e and \tilde{B} at $r/a = 0.85$. Similar to Fig. 6, peaks in coherence have been observed at tearing mode frequencies and at high frequencies. The feature at high frequencies is only present in the coherence involving \tilde{B}_{\parallel} . When paired with a near-zero cross phase in this high frequency range, these features suggest a compressive nature for this unidentified mode.

filtered with $f \geq 60$ kHz), are consistent with drift wave theory (where $\tilde{n}_e/n_e \geq e\tilde{V}_f/k_B T_e$ is expected³³).

The same two coherence features visible in Fig. 6(a) are also present in the coherence of magnetic field components with both \tilde{V}_f and \tilde{n}_e , as seen in Figs. 7 and 8, respectively. While the low-frequency feature associated with the tearing modes is always present, the high-frequency peak is present in correlations involving \tilde{B}_{\parallel} but not \tilde{B}_{\perp} . The elevated coherence between \tilde{n}_e and \tilde{B}_{\parallel} suggests a compressive nature for the high frequency fluctuations and this is further supported by the near-zero cross phase between \tilde{n}_e and \tilde{B}_{\parallel} (Fig. 7(b)). Note that, while a high-frequency peak is clearly present in coherence plots, only a slight “knee” is apparent near these frequencies in the magnetic and kinetic frequency power spectra (Fig. 5). It was previously shown that the magnetic spectrum is well-fit by a dissipative turbulence model, so it is unclear whether the slight “knee” near 100 kHz is related

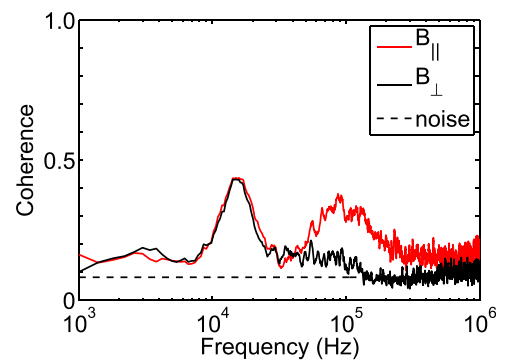


FIG. 8. Coherences have been measured between \tilde{V}_f and \tilde{B} at $r/a = 0.85$. As before, there is a peak in the coherence at tearing mode frequencies and a second peak (involving \tilde{B}_{\parallel}) at high frequencies. Note that we have not included plots of coherences between various magnetic field components. For pairs of magnetic field components, coherence is very high for all but the highest frequencies.

to drift wave activity or whether it might indicate onset of dissipation.^{4,34,35}

The $\tilde{V}_f, \tilde{B}_{\parallel}$ coherence for the high-frequency fluctuations has radial dependence, peaking at $r \approx 43$ cm as shown in Fig. 9. While this is near the magnetic reversal surface, the gradients in the density and temperature profiles (which are the source of free energy for drift waves) are at the maximum in this region of standard RFP plasmas. The density profile measured in similar low current plasmas is provided to illustrate this gradient.³⁶

Assuming that the measured quantities (such as \tilde{B}_{\parallel} and \tilde{V}_f) have similar spatial structures at frequencies where the coherence is high, measurements of B_{\parallel} at one location and two measurements of V_f (spaced in the perpendicular direction) can be used to find $\tilde{V}_f(k_{\perp}, f)$ and $\tilde{B}_{\parallel}(k_{\perp}, f)$. This then allows the coherence between the two quantities to be found in the standard way for each (k_{\perp}, f) bin. As this analysis results in a different level of statistical significance for each (k_{\perp}, f) bin, the coherence is normalized by its bin-specific minimum level of statistical significance to better highlight areas of strong correlation. The result of this analysis is shown in Fig. 10.

The high-frequency coherence peak is readily apparent in Fig. 10 and is associated with $k_{\perp} = -0.25 \pm 0.10$ cm⁻¹ and $f = 80 \pm 20$ kHz. This frequency and wavenumber correspond to a wave propagating in the electron diamagnetic drift direction with a phase speed of $v_{ph} = 2.0 \times 10^6 \pm 0.9 \times 10^6$ cm/s, which is approximately $0.4c_s \approx 0.01v_A$ where v_A and c_s are the Alfvén and ion acoustic speeds, respectively. This is close to the expected value for drift waves $v_{De} = \omega_{*e}/k_{\perp} = T_e/(eBL_n) = \rho_s c_s/L_n$, where ω_{*e} is the electron diamagnetic drift frequency. The local density-gradient-scale length is $L_n \approx 2$ cm, and the ion acoustic gyroradius $\rho_s = c_s/\omega_{ci} \approx \rho_i = 0.8$ cm; hence, $v_{De} \approx 0.4c_s$.

The temporal evolution for the sawtooth cycle is resolved using short-time Fourier transform analysis (STFT), shown in Fig. 11 for the coherence between \tilde{V}_f and \tilde{B}_{\parallel} as well as between \tilde{n}_e and \tilde{B}_{\parallel} . The coherence at the tearing mode frequencies (~ 20 kHz) increases in advance of the

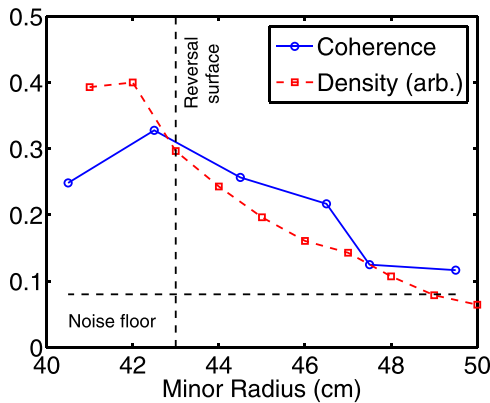


FIG. 9. The maximum coherence for $f \approx 80$ kHz between \tilde{B}_{\parallel} and \tilde{V}_f versus minor radius. The shape of the coherence spectrum varies modestly at different minor radii, and so its local maximum values are plotted here for simplicity. The density profile³⁶ is plotted to show that the coherence is highest near the toroidal field reversal surface where the density gradient is near maximum.

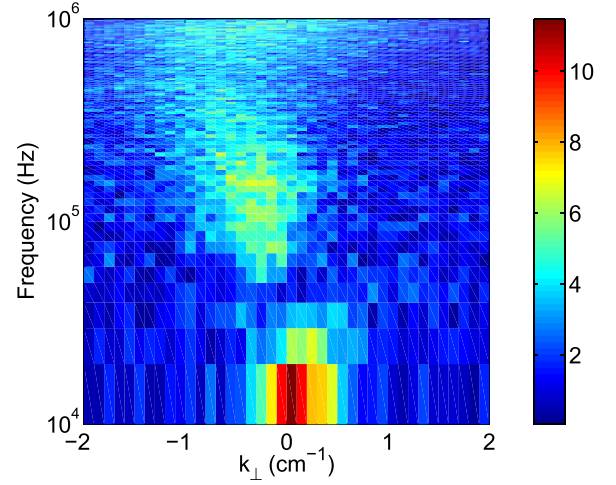


FIG. 10. A two point correlation technique has been extended to provide a measurement of normalized coherence between \tilde{V}_f and \tilde{B}_{\parallel} as a function of frequency and perpendicular wavenumber at $r/a = 0.85$. Using this information, the phase velocity for the peak of interest is $v_{ph} \approx 2 \times 10^6$ cm/s in the electron diamagnetic drift direction.

sawtooth crash, subsides during the crash, and then recovers on the sawtooth period timescale, which is several ms. In contrast, the coherence for the high frequency peak ~ 80 kHz is reduced only temporarily during the violent crash phase.

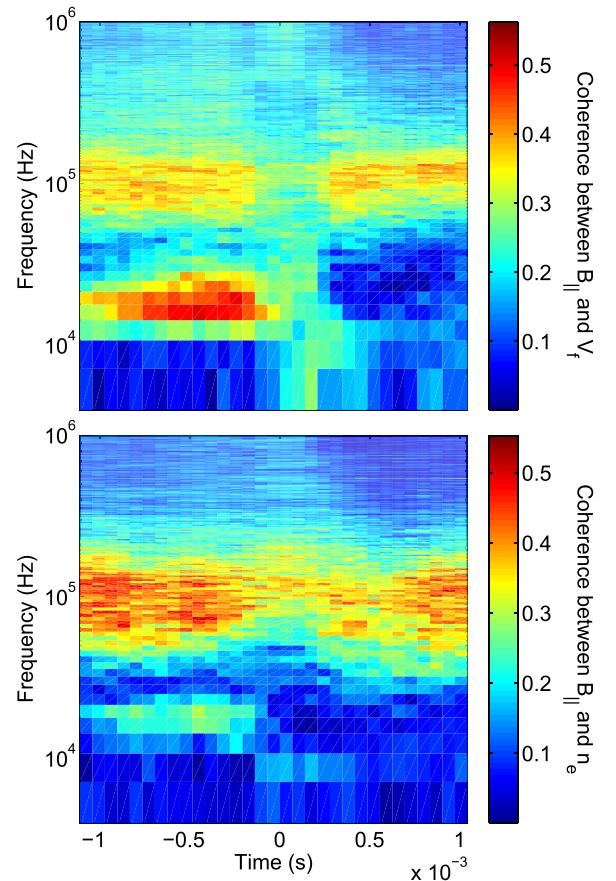


FIG. 11. Time-frequency analysis of the coherence between \tilde{B}_{\parallel} and \tilde{V}_f (top) and \tilde{n}_e (bottom) reveals the temporal behavior of these coherence peaks through a sawtooth cycle. While strong coherence associated with tearing modes (near 20 kHz) takes some time to return after a sawtooth event, the high-frequency coherence peak (near 80 kHz) returns almost immediately. Measurements were collected at $r/a = 0.85$.

In fact, after the crash, the strongest coherence occurs in this part of the frequency spectrum. This suggests that the high frequency turbulence is not simply dependent on the dynamics of the dominant tearing modes, even though the energy in the turbulence rises and falls in concert with the tearing mode amplitude.

V. DISCUSSION

The measurements described above suggest that the drift waves are an energetic component of the turbulent cascade at small scales and high frequencies. The wavelength and speed have appropriate values for drift waves, the coherence is at maximum where the gradients in density and temperature are large, and the kinetic energy begins to dominate the magnetic energy at the drift wave scale. While other wave modes have been examined, none have been identified that are consistent with the observations presented here. The slow mode, a compressive mode present in solar wind turbulence,²⁸ has a phase speed that is much smaller than c_s when propagating perpendicular to \mathbf{B}_0 and should show anticorrelation between \tilde{V}_f and \tilde{n}_e (unlike the correlation we observe). Flow driven modes have also been considered, as sheared $E \times B$ flow is present in MST plasmas. While an exhaustive collection of flow measurements is not available, all previous evidence has shown that conditions are not favorable for flow-driven instabilities, even when operating in modes with increased velocity shear.³⁷

The energy source for these drift waves is unknown. It is not clear if they are excited by nonlinear coupling to the tearing-driven Alfvénic cascade or are an independent instability. The energy in the turbulent spectrum rises and falls in concert with the sawtooth cycle, suggesting a direct connection with the dominant tearing modes, but the coherence at high frequencies is more persistent than for the tearing modes, suggesting the possibility of independent instability.

Gyrokinetic studies have been performed for improved-confinement MST plasma equilibria, motivated by the likelihood that drift waves are important for transport when tearing is greatly reduced.^{18,19} Many of the standard drift wave modes can be unstable. Fluctuation measurements in these improved-confinement MST plasmas show clear evidence for an unstable density-gradient-driven TEM that has a density-gradient threshold and peaks in the strong gradient region of the plasma.²¹ The large reduction in broadband turbulence when tearing instability is reduced makes the TEM readily visible. Gyrokinetic studies have not yet been performed for standard RFP plasma equilibria, but the gradients in the edge region are comparable to those attained in improved-confinement conditions.³⁸

Drift waves have been most extensively studied for low β plasmas where they are essentially electrostatic and not associated with fluctuating magnetic fields. At small finite values of β they acquire a magnetic fluctuation component mostly associated with parallel fluctuating current density,³⁹ resulting in \tilde{B}_\perp but not \tilde{B}_\parallel . While there is a compressional mode of the drift wave with $\tilde{B}_\parallel = k_\perp \tilde{E}_r / \omega$ (the coupled Alfvén-drift wave), it has a dispersion relation that leads to a

wave speed much faster than observed in our experiments.⁴⁰ Gyrokinetic analysis of reconnection in the presence of gradients has led to the identification of the gradient-driven-drift-coupling (GDC) instability that accesses gradient free energy through parallel field fluctuations.⁴¹ This instability arises in magnetic field configurations with weak or no magnetic shear and has not figured in most previous analyses of drift waves. There is evidence that it is unstable in the large plasma device.⁴² While it is not likely to be unstable in the strongly-sheared RFP, it may arise as a subdominant stable mode excited by the turbulence, analogous to the subdominant microtearing mode excited in ITG turbulence.⁴³ The coupling of drift motions to parallel magnetic field fluctuations in the GDC instability makes it relevant to observations described above and will be investigated further. The relatively weak correlations of electrostatic fluctuations with \tilde{B}_\perp seen in MST plasmas could indicate that the perpendicular magnetic field energy is dominated by the Alfvénic component of the turbulent cascade.

VI. SUMMARY

Broadband turbulent electric field fluctuations in the edge region of standard MST plasmas have been characterized. Like magnetic fluctuations (at high frequencies), electric field turbulence is highly anisotropic with power spread broadly in a direction perpendicular to the strong guide field. Due to the sheared magnetic field profile, this anisotropy indicates a short radial coherence length associated with these fluctuations.

Magnetic field spectra are steeper than electric field spectra, with magnetic fluctuations containing more power at low frequencies, while kinetic $\tilde{\mathbf{E}} \times \mathbf{B}_0$ fluctuations contain more power at high frequencies. Coherence measurements were used to examine further the geometry and properties of high-frequency modes mediating the turbulent cascade. A high-frequency peak was apparent when examining coherences between \tilde{B}_\parallel and fluctuating electrostatic quantities, \tilde{V}_f and \tilde{n}_e , indicating a mode with a compressive nature. Two-point correlation techniques were extended to examine the frequency-wavenumber coherence measurement, allowing the phase velocity $v_{ph} \approx 0.4c_s \ll v_A$ in the electron diamagnetic drift direction to be determined.

The observed features suggest drift waves are an energetic component of the high frequency turbulence. It is not yet clear if they are excited in a generalization of the tearing-driven Alfvénic cascade or if they reflect independent instability. The relatively weak correlations of electrostatic fluctuations with \tilde{B}_\perp could indicate that the perpendicular magnetic field energy is dominated by the Alfvénic component of the turbulent cascade. Further investigation is necessary to determine the exact type of drift wave that is present.

SUPPLEMENTARY MATERIAL

See [supplementary material](#) for all MST data shown in this paper, in addition to an appendix providing details of the two-point correlation technique and extensions discussed in this manuscript.

ACKNOWLEDGMENTS

This material is based upon work supported by the U.S. Department of Energy Office of Science, Office of Fusion Energy Sciences program under Award No. DE-FC02-05ER54814 and the National Science Foundation under Grant No. PHY 08-2189.

- ¹S. Ortolani and D. Schnack, *Magneto-hydrodynamics of Plasma Relaxation* (World Scientific, 1993).
- ²Y. L. Ho and G. G. Craddock, *Phys. Fluids* **3**, 721 (1991).
- ³A. Kuritsyn, G. Fiksel, A. F. Almagri, D. L. Brower, W. X. Ding, M. C. Miller, V. V. Mirnov, S. C. Prager, and J. S. Sarff, *Phys. Plasmas* **16**, 055903 (2009).
- ⁴Y. Ren, A. F. Almagri, G. Fiksel, S. C. Prager, J. S. Sarff, and P. W. Terry, *Phys. Rev. Lett.* **107**, 195002 (2011).
- ⁵P. S. Iroshnikov, *Astron. Zh.* **40**, 742 (1963).
- ⁶R. H. Kraichnan, *Phys. Fluids* **8**, 1385 (1965).
- ⁷P. Goldreich and S. Sridhar, *Astrophys. J.* **438**, 763 (1995).
- ⁸P. W. Terry, C. McKay, and E. Fernandez, *Phys. Plasmas* **8**, 2707 (2001).
- ⁹S. Boldyrev, *Astrophys. J.* **626**, L37 (2005).
- ¹⁰G. G. Howes, W. Dorland, S. C. Cowley, G. W. Hammett, E. Quataert, A. A. Schekochihin, and T. Tatsuno, *Phys. Rev. Lett.* **100**, 065004 (2008).
- ¹¹J. S. Sarff, A. F. Almagri, J. K. Anderson, T. M. Biewer, A. P. Blair, M. Cengher, B. E. Chapman, P. K. Chattopadhyay, D. Craig, D. J. Den Hartog, F. Ebrahimi, G. Fiksel, C. B. Forest, J. A. Goetz, D. Holly, B. Hudson, T. W. Lovell, K. J. McCollam, P. D. Nonn, R. O'Connell, S. P. Oliva, S. C. Prager, J. C. Reardon, M. A. Thomas, M. D. Wyman, D. L. Brower, W. X. Ding, S. D. Terry, M. D. Carter, V. I. Davydenko, A. A. Ivanov, R. W. Harvey, R. I. Pinsker, and C. Xiao, *Nucl. Fusion* **43**, 1684 (2003).
- ¹²D. F. Escande, P. Martin, S. Ortolani, A. Buffa, P. Franz, L. Marrelli, E. Martinez, G. Spizzo, S. Cappello, A. Murari, R. Pasqualotto, and P. Zanca, *Phys. Rev. Lett.* **85**, 1662 (2000).
- ¹³R. Lorenzini, E. Martinez, P. Piovesan, D. Terranova, P. Zanca, M. Zuin, A. Alfier, D. Bonfiglio, F. Bonomo, A. Canton, S. Cappello, L. Carraro, R. Cavazzana, D. F. Escande, A. Fassina, P. Franz, M. Gobbin, P. Innocente, L. Marrelli, R. Pasqualotto, M. E. Puiatti, M. Spolaore, M. Valisa, N. Vianello, and P. Martin, *Nat. Phys.* **5**, 570 (2009).
- ¹⁴F. Sattin, X. Garbet, and S. C. Guo, *Plasma Phys. Controlled Fusion* **52**, 105002 (2010).
- ¹⁵I. Predebon, C. Angioni, and S. C. Guo, *Phys. Plasmas* **17**, 012304 (2010).
- ¹⁶I. Predebon, L. Carraro, and C. Angioni, *Plasma Phys. Controlled Fusion* **53**, 125009 (2011).
- ¹⁷D. Carmody, M. J. Pueschel, and P. W. Terry, *Phys. Plasmas* **20**, 052110 (2013).
- ¹⁸D. Carmody, M. J. Pueschel, J. K. Anderson, and P. W. Terry, *Phys. Plasmas* **22**, 012504 (2015).
- ¹⁹P. W. Terry, D. Carmody, H. Doerk, W. Guttenfelder, D. R. Hatch, C. C. Hegna, A. Ishizawa, F. Jenko, W. M. Nevins, I. Predebon, M. J. Pueschel, J. S. Sarff, and G. G. Whelan, *Nucl. Fusion* **55**, 104011 (2015).
- ²⁰M. Zuin, S. Spagnolo, I. Predebon, F. Sattin, F. Auriemma, R. Cavazzana, A. Fassina, E. Martinez, R. Paccagnella, M. Spolaore, and N. Vianello, *Phys. Rev. Lett.* **110**, 055002 (2013).
- ²¹J. Duff, B. Chapman, J. Sarff, P. Terry, Z. Williams, W. Ding, D. Brower, and E. Parke, *Bull. Am. Phys. Soc.* **60** (2015), see <http://meetings.aps.org/link/BAPS.2015.DPP.CP12.27>.
- ²²J. W. Belcher and L. Davis, Jr., *J. Geophys. Res.* **76**, 3534, doi:10.1029/JA076i016p03534 (1971).
- ²³W. H. Matthaeus, M. L. Goldstein, and D. A. Roberts, *J. Geophys. Res.* **95**, 20673, doi:10.1029/JA095iA12p20673 (1990).
- ²⁴J. J. Podesta, D. A. Roberts, and M. L. Goldstein, *Astrophys. J.* **664**, 543 (2007).
- ²⁵J. A. Tessein, C. W. Smith, B. T. MacBride, W. H. Matthaeus, M. A. Forman, and J. E. Borovsky, *Astrophys. J.* **692**, 684 (2009).
- ²⁶C. H. K. Chen, S. D. Bale, C. Salem, and F. S. Mozer, *Astrophys. J.* **737**, L41 (2011).
- ²⁷S. Boldyrev, J. C. Perez, J. E. Borovsky, and J. J. Podesta, *Astrophys. J.* **741**, L19 (2011).
- ²⁸G. G. Howes, S. D. Bale, K. G. Klein, C. H. K. Chen, C. S. Salem, and J. M. TenBarge, *Astrophys. J. Lett.* **753**, L19 (2012).
- ²⁹S. Choi, D. Craig, F. Ebrahimi, and S. C. Prager, *Phys. Rev. Lett.* **96**, 145004 (2006).
- ³⁰J. M. Beall, Y. C. Kim, and E. J. Powers, *J. Appl. Phys.* **53**, 3933 (1982).
- ³¹J. S. Sarff, S. Assadi, A. F. Almagri, M. Cecik, D. J. den Hartog, G. Fiksel, S. A. Hokin, H. Ji, S. C. Prager, W. Shen, K. L. Sidikman, and M. R. Stoneking, *Phys. Fluids B* **5**, 2540 (1993).
- ³²A. Kolmogorov, *Dokl. Akad. Nauk SSSR* **30**, 301 (1941).
- ³³D. L. Jassby, *Phys. Fluids* **15**, 1590 (1972).
- ³⁴P. W. Terry and V. Tangri, *Phys. Plasmas* **16**, 082305 (2009).
- ³⁵P. W. Terry, A. F. Almagri, G. Fiksel, C. B. Forest, D. R. Hatch, F. Jenko, M. D. Nornberg, S. C. Prager, K. Rahbarnia, Y. Ren, and J. S. Sarff, *Phys. Plasmas* **19**, 055906 (2012).
- ³⁶M. C. Miller, "Non-axisymmetric flows and transport in the edge of MST," Ph.D. thesis (The University of Wisconsin, Madison, 2011).
- ³⁷B. E. Chapman, C.-S. Chiang, S. C. Prager, J. S. Sarff, and M. R. Stoneking, *Phys. Rev. Lett.* **80**, 2137 (1998).
- ³⁸B. E. Chapman, A. F. Almagri, J. K. Anderson, T. M. Biewer, P. K. Chattopadhyay, C.-S. Chiang, D. Craig, D. J. Den Hartog, G. Fiksel, C. B. Forest, A. K. Hansen, D. Holly, N. E. Lanier, R. O'Connell, S. C. Prager, J. C. Reardon, J. S. Sarff, M. D. Wyman, D. L. Brower, W. X. Ding, Y. Jiang, S. D. Terry, P. Franz, L. Marrelli, and P. Martin, *Phys. Plasmas* **9**, 2061 (2002).
- ³⁹J. D. Callen, *Phys. Rev. Lett.* **39**, 1540 (1977).
- ⁴⁰W. Horton, *Turbulent Transport in Magnetized Plasmas* (World Scientific, 2012).
- ⁴¹M. J. Pueschel, P. W. Terry, D. Told, and F. Jenko, *Phys. Plasmas* **22**, 062105 (2015).
- ⁴²M. J. Pueschel, G. Rossi, D. Told, P. W. Terry, F. Jenko, and T. A. Carter, *Plasma Phys. Controlled Fusion* **59**, 024006 (2017).
- ⁴³D. R. Hatch, M. J. Pueschel, F. Jenko, W. M. Nevins, P. W. Terry, and H. Doerk, *Phys. Rev. Lett.* **108**, 235002 (2012).